Available online at www.sciencedirect.com
SCIENCE DIRECT®
ELSEVIER
International Journal of Solids and Structures 42 (2005) 3744–3772
INTERNATIONAL JOURNAL OF SOLIDS and STRUCTURES
www.elsevier.com/locate/ijsolstr

A thermodynamics based damage mechanics constitutive model for low cycle fatigue analysis of microelectronics solder joints incorporating size effects

Juan Gomez *, Cemal Basaran

UB Electronic Packaging Laboratory, Civil Engineering, University at Buffalo, 102 Ketter Hall, Buffalo, NY 14260, USA

Received 27 August 2004; received in revised form 19 November 2004
Available online 21 January 2005

Abstract

Below certain length scales and in the presence of a non-uniform plastic strain field the mechanical behavior of many metals and its alloys is substantially different from that in bulk specimens. In particular, an increase in resistance with decreasing size has been observed in Pb/Sn eutectic solder alloys which are extensively used in microelectronics packaging interconnects. Due to the high homologous temperature, the Pb/Sn solder exhibits creep–fatigue interaction and significant time, temperature, stress and rate dependent material characteristics. The simultaneous consideration of all the above mentioned factors makes constitutive modeling an extremely difficult task. In this paper, a viscoplastic constitutive model unified with a thermodynamics based damage evolution model is embedded into a couple stress framework in order to simulate low cycle fatigue response coupled to size effects. The model is implemented into commercial finite element code ABAQUS. The microbending experiment on thin nickel foils is used to validate the model. Analyses are performed on a thin layer solder joint in bending under cyclic loading conditions.

Keywords: Finite element analysis; Constitutive modeling; Strain gradient plasticity; Low cycle fatigue; Damage mechanics; Solder joints

1. Introduction

Recent developments in the electronics industry have shown a steady and increasing tendency towards miniaturization. Some examples are the cases of thin films, sensors, actuators and micro–electro

* Corresponding author. Tel.: +1 7168360107; fax: +1 7166453733.
E-mail address: jdg8@buffalo.edu (J. Gomez).

0020-7683/$ - see front matter © 2004 Elsevier Ltd. All rights reserved.
doi:10.1016/j.ijsolstr.2004.11.022

mechanical systems where the entire system size can be less than 10 μm (Xue, 2001). At the same time, there exists vast experimental evidence that the mechanical properties of some materials at such small scales are substantially different than those of bulk specimens (Lloyd, 1994; Fleck et al., 1994; Poole et al., 1996). In the elastic regime, size effects are generally present at length scales of the order of interatomic distances (Mindlin, 1964). In the presence of non-uniform plastic strains, size effects can be triggered at much larger length scales than in atomic dimensions. Fleck and Hutchinson (1993) have shown that the torsional strength of thin copper wires increases as the wire diameter decreases from 170 μm to 12 μm. During nanoindentation experiments on copper specimens McElhaney et al. (1998) identified a dependence of the measured hardness on the indentation depth. Stolken and Evans (1998) found a dependence of the bending moment on the thickness as the beam thickness went from 50 μm to 12.5 μm on thin nickel microbeams. Xue et al. (2001) addressed the problem of an aluminum matrix reinforced by small silicon carbide particles. It was observed that for a constant particle volume fraction, significant increase in the resistance was obtained when the particle diameter went from 16.0 μm to 7.5 μm. The above phenomena exhibits size effects due to the presence of a non-uniform plastic deformation. In contrast, Bonda and Noyan (1996) studied size effects when the specimen size is smaller than the representative volume element (RVE) of the material for the particular case of Pb/Sn solder alloys. The latter class of size effects are present even under uniform deformation modes. In this work the focus is on the first set of size dependent behavior. Fleck and Hutchinson (1993, 1997) have promulgated the existence of a plastic material length scale that explains the size effects. When typical structural dimensions (for instance, the beam thickness in microbeams, indentation depth in nanoindentation, wire diameter in microtorsion) approach this intrinsic length scale, the density of geometrically necessary dislocations (described in terms of strain gradients) becomes comparable to the density of statistically stored dislocations (described in terms of plastic strains). Based on this phenomenological argument Fleck and Hutchinson (1993, 1997) have pioneered the development of a strain gradient plasticity theory. The density of geometrically necessary dislocations is explained as an extra amount of dislocations that are required to satisfy displacement compatibility conditions within the material (Nye, 1953). According to this line of thought, having additional dislocations hardens the material further and as a result at smaller scales materials are stronger. Consideration of the density of geometrically necessary dislocations into plasticity models has been accomplished mainly by means of two theories. First, by a general solid continuum model where all the gradients of the displacement gradient tensor (strains and rotations) are considered. This model falls within the type of solids considered by Toupin (1962) and Mindlin (1965) where higher order stresses appear as work conjugates to the second order displacement gradients. The other approach is where only the rotation gradients (curvatures) are considered. This theory falls within the type of solid continuum considered by Cosserat and Cosserat (1909) and termed couple stress theory (CS) or Cosserat continuum. In a CS solid the transmission of loads on both sides of an infinitesimal surface element dS is represented in terms of a couple vector in addition to the force vector used in the classical theory. In this theory the curvatures appear naturally as work conjugates to the couple stresses providing a physically sound framework for the consideration of the geometrically necessary dislocations. The work presented in this paper is based on the Fleck and Hutchinson (1993) couple stress solid. Nanoindentation experiments conducted on Pb/Sn solder joints at the University at Buffalo Electronics Packaging Lab reveal the presence of size effects (see Fig. 1). Solder joints in electronic packaging fail due to the combined effects of creep and thermo mechanical fatigue due to the coefficient of thermal expansion mismatch between the soldered parts. All these factors coupled to the known size effects should be included in a constitutive model for fatigue failure analysis of solder joints (Basaran and Yan, 1998; Basaran et al., 2004). Basaran and Tang (2002) have proposed a damage mechanics based unified constitutive model where damage evolution is described in terms of entropy production. The model has been extensively verified against experimental results. The purpose of this work is to incorporate size effects into the Basaran damage mechanics model making

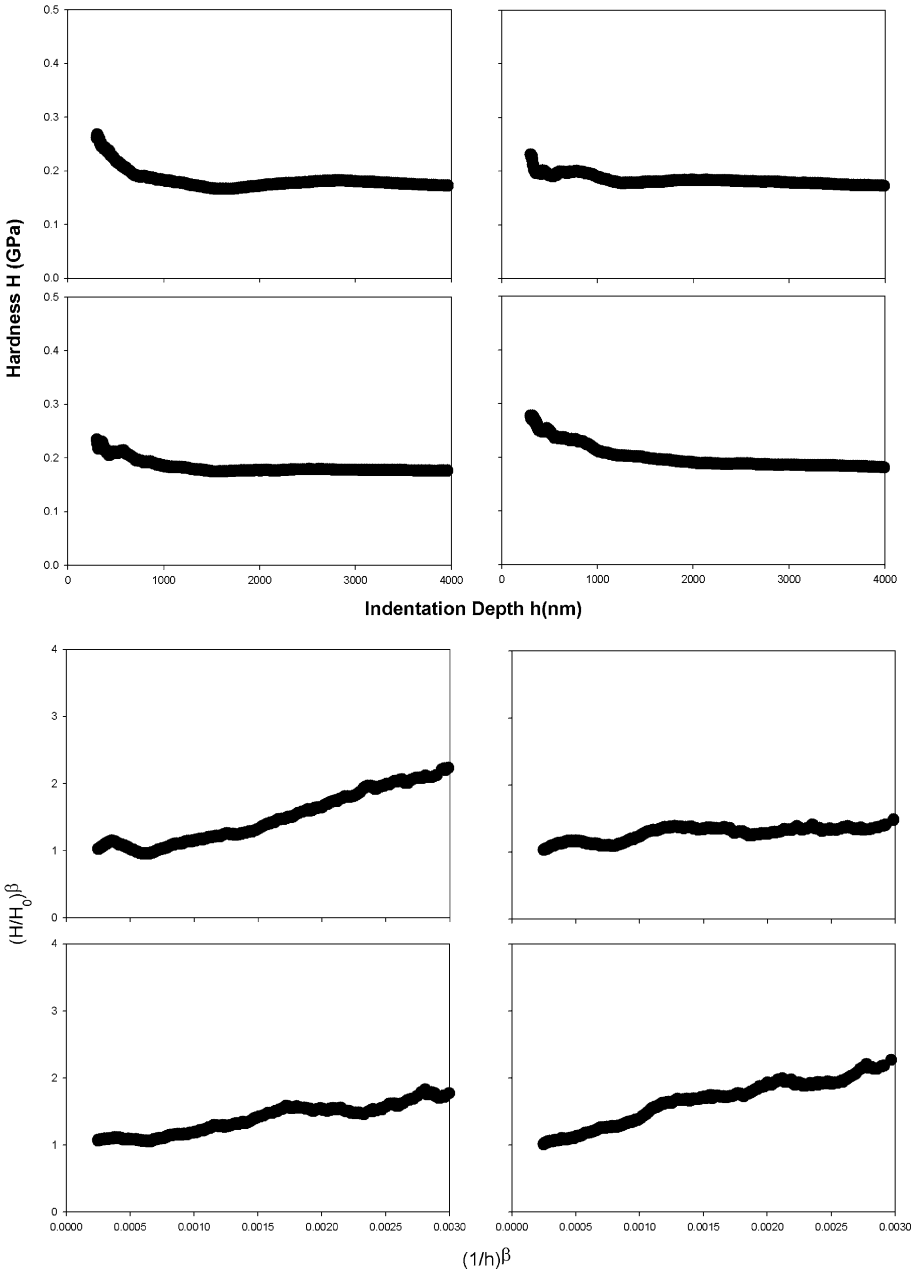

Fig. 1. Nano indentation of Pb/Sn solder alloy.

use of Fleck and Hutchinson (1993) couple stress based strain gradient plasticity theory (CS-SGPT). To be able to unify CS-SGPT with a damage mechanics model the existing strain gradient theory has to be generalized in order to consider damage and rate dependent effects under low cycle fatigue conditions. In this regard, it is worth mentioning that the formulation of length scale plasticity theories has been

driven mainly, by the availability of experimental setups at small scales. Namely, the nanoindentation, microtorsion and microbending experiments, where conditions of proportional loading are present and deformation theory versions of the models are capable of describing the experiments. For path dependent problems a flow theory description of the constitutive model is needed. In this work, we modify the Fleck and Hutchinson (1993) couple stress strain gradient plasticity theory from deformation theory to flow theory in order to embed our unified damage mechanics based thermodynamics framework.

The finite element implementation of the problem presents two major challenges. Firstly, the presence of second order displacement gradients creates the need for elements of C^1 compatibility in a displacement based formulation. Alternatively, C^0 continuous elements can be used based on mixed variational principles like in Xia and Hutchinson (1996), Herrmann (1983) and Begley and Hutchinson (1998). Secondly, in a finite element implementation the incremental stress–strain relations are written in rate form and the model needs to be time integrated in order to advance the solution along a time step. Herein, we follow the approach suggested by Shu and Fleck (1999) where a generalized couple stress theory is used as the basis for a penalty/reduced integration finite element formulation. This allows the consideration of rotations like independent degrees of freedom. Compatibility between translational and rotational degrees of freedom is then enforced through a penalty parameter. Alternatively, mixed approaches can be used, where the kinematic constraint is enforced by some Lagrange multiplier technique. For the integration algorithm we use a return mapping scheme analogous to the one presented by Simo and Hughes (1998). The paper is organized as follows. Section 2 presents a brief description of the Cosserat couple stress theory in terms of equilibrium equations and boundary conditions and the general equivalent plastic strain definition with the addition of the strain gradients defined here in terms of curvatures. Next, we use the approach from Abu Al-Rub and Voyiadjis (2004) to determine a preliminary value of the length scale using nanoindentation experiment. In the majority of the cases, the length scale has been determined based on curve fitting of computational results to experimental data (Yuan and Chen, 2001; Begley and Hutchinson, 1998; Nix and Gao, 1998). In few additional contributions the length scale has been measured from microbending experiments (Stolken and Evans, 1998; Shrotriya et al., 2003). Recently, Abu Al-Rub and Voyiadjis (2004) proposed a methodology to determine the length scale using results from nanoindentation experiments based on the Taylor hardening model from dislocation mechanics and on a model that accounts for the density of geometrically necessary dislocations underneath a nanoindenter. Recently Gomez et al. (submitted for publication) reported a nanoindentation study on Pb/Sn microelectronics solder joints to find the length scale and to show how this material in fact exhibits size effects. The additional Pb/Sn material parameters were determined by Tang (2002) based on thermomechanical fatigue experiments on microelectronics size solder joints. The next section presents the finite element formulation and the proposed constitutive model together with the return mapping scheme used to integrate the rate form of the constitutive equations. Here it is shown that the penalty function treatment of the problem is equivalent to considering a general Cosserat solid where an additional "material parameter" takes the form of a penalty number as implemented by Shu and Fleck (1999). The last section describes the numerical simulations. In a bending problem the strain gradients (corresponding to curvatures) are expected to be enough to capture the size dependent response. This justifies the use of a couple stress solid. The experimental results of Stolken and Evans on microbending of thin nickel beams are simulated using the proposed model. In the following section we study the problem of a thin cantilever beam made out of Pb/Sn alloy, under cyclic mechanical loading conditions. In order to capture the influence of the length scale on damage, results are shown in terms of stress strain hysteresis loops and evolution of the damage parameter for different assumed values of the length scale. In the final section we identify the needs for further improvement of the proposed model.

2. Review of Cosserat couple stress theory and length scale interpretation

2.1. Couple stress theory

In the following discussion repeated indices are assumed to follow the summation convention unless explicitly stated otherwise. e_{ijk} is the alternating tensor, δ_{ij} is the identity tensor and a comma represents a derivative with respect to Cartesian coordinates. There are different interpretations of Cosserat continuum. In the following part we discuss our point of view which is necessary for presenting our model effectively. In Cosserat and Cosserat (1909) couple stress theory a differential material element admits not only normal and shear but also couple stress components as shown in Fig. 2. For linear elastic behavior the usual stress components are functions of the strains and the couple stresses are functions of the strain gradients. Two distinct theories are identified in the work of the Cosserats. First, there is a reduced couple stress theory with the kinematic quantities being the displacement u_i and an associated material rotation θ_i tied to the displacements by the kinematic constraint (1) and with the definitions of strain and curvatures expressed in (2) and (3).

$$\theta_i = \frac{1}{2} e_{ijk} u_{k,j} \tag{1}$$

$$\varepsilon_{ij} = \frac{1}{2}(u_{i,j} + u_{j,i}) \tag{2}$$

$$\chi_{ij} = \theta_{i,j} \tag{3}$$

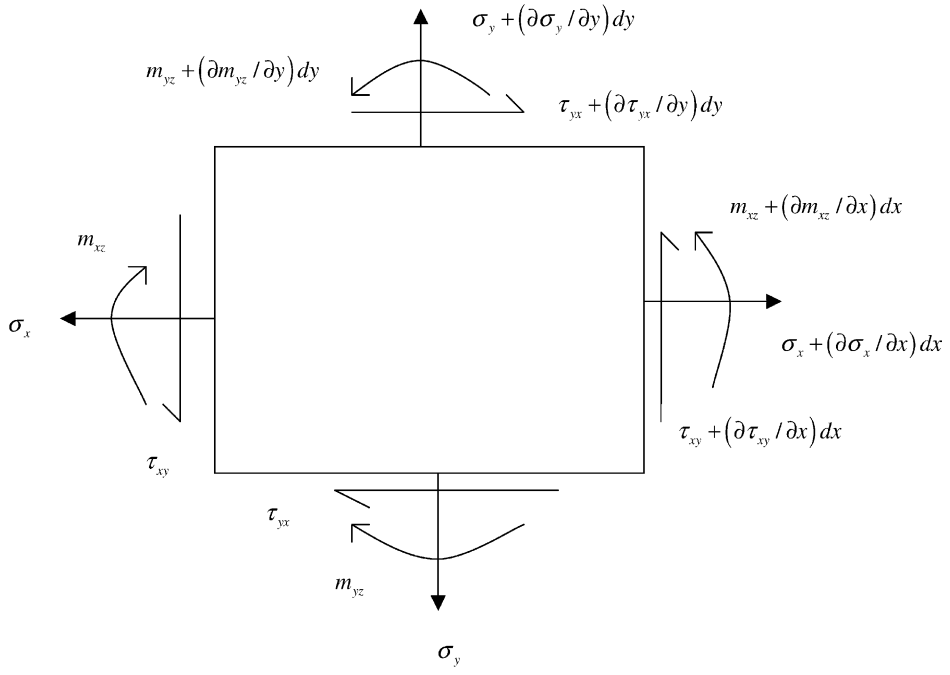

Fig. 2. The Cosserat couple stress block.

Second, there is a general couple stress theory in terms of a microrotation ω_i which is regarded as an independent kinematic variable. The rotation and microrotation are related by a relative rotation tensor $\alpha_{ij} = e_{ijk}\omega_k - e_{ijk}\theta_k$. For the particular choice of $\omega_k = \theta_k$ the general couple stress theory reduces to the reduced couple stress theory. Equilibrium of the differential element shown in Fig. 2, after neglecting body forces and body couples yields

$$\sigma_{ji,j} + \tau_{ji,j} = 0 \tag{4}$$

$$\tau_{jk} + \frac{1}{2} e_{ijk} m_{\mathrm{pi,p}} = 0 \tag{5}$$

where σ_{ij} and τ_{ij} are the symmetric and anti-symmetric components of the Cauchy stress tensor respectively, and m_{ij} is the couple stress tensor. Surface stress tractions and surface couple stress tractions are given:

$$t_i = (\sigma_{ij} + \tau_{ij}) n_j \tag{6}$$

$$q_i = m_{ij} n_j \tag{7}$$

where t_i is the traction vector, q_i is the couple tractions vector and n_i is a surface outward normal vector. Herrmann (1983), Fleck and Hutchinson (1993), and Xia and Hutchinson (1996) among others have used the theory with the constraint (1) in several problems, while de Borst (1993) and Pamin (1994) have used the original Cosserat theory to solve deformation localization problems. For the case of elastic material behavior, the Cosserat couple stress solid can be obtained after postulating a strain energy density function dependent on strains and curvatures (rotation gradients). Toupin (1962) and Mindlin (1965) extended this theory to include also stretch gradients. In particular, they considered invariants of the strain and strain gradients into the strain energy density function in terms of the following generalized Von Mises strain invariant which is written here after Fleck and Hutchinson (1997),

$$E^2 = \frac{2}{3}\varepsilon'_{ij}\varepsilon'_{ij} + c_1 \eta'_{iik}\eta'_{jjk} + c_2 \eta'_{ijk}\eta'_{ijk} + c_3 \eta'_{ijk}\eta'_{kij} \tag{8}$$

In (8), a prime superscript denotes deviatoric component, $\eta_{ijk} = u_{k,ij}$ are the strain gradients and the c'_i s are additional material constants with dimensions length square (L^2). Eq. (8) is the basis for the most general strain gradient plasticity theory and essentially reveals the phenomenological coupling between the densities of statistically and geometrically stored dislocations. The reduced couple stress theory is just a particular instance of (8) where only rotation gradients are considered as explained below.

2.2. Length scale interpretation

Introducing the following set of length scales

$$\begin{aligned} l_1^2 &= c_2 + c_3 \\ l_2^2 &= c_2 - \frac{1}{2} c_3 \\ l_3^2 &= \frac{5}{2} c_1 + c_2 - \frac{1}{4} c_3 \end{aligned} \tag{9}$$

and following Smyshlyaev and Fleck (1996) Eq. (8) can be re-written in the following form which results after performing an orthogonal decomposition

$$E^2 = \frac{2}{3}\varepsilon'_{ij}\varepsilon'_{ij} + l_1^2 \eta^{(1)}_{ijk}\eta^{(1)}_{ijk} + l_2^2 \eta^{(2)}_{ijk}\eta^{(2)}_{ijk} + l_3^2 \eta^{(3)}_{ijk}\eta^{(3)}_{ijk} \tag{10}$$

This expression can be further simplified making explicit the connection between the strain gradients and the curvatures

$$E^2 = \frac{2}{3}\varepsilon'_{ij}\varepsilon'_{ij} + l_1^2\eta^{(1)}_{ijk}\eta^{(1)}_{ijk} + \frac{2}{3}\left(2l_2^2 + \frac{12}{5}l_3^2\right)\chi_{ij}\chi_{ij} + \frac{2}{3}\left(2l_2^2 - \frac{12}{5}l_3^2\right)\chi_{ij}\chi_{ji} \tag{11}$$

Letting

$$\begin{aligned} l_{\mathrm{SG}}^2 &= l_1^2 \\ l_{\mathrm{CS}}^2 &= 2l_2^2 + \frac{12}{5}l_3^2 \\ l_{\mathrm{in}}^2 &= 2l_2^2 - \frac{12}{5}l_3^2 \end{aligned} \tag{12}$$

(11) can be written like

$$E^2 = \frac{2}{3}\varepsilon'_{ij}\varepsilon'_{ij} + l_{\mathrm{SG}}^2\eta^{(1)}_{ijk}\eta^{(1)}_{ijk} + \frac{2}{3}l_{\mathrm{CS}}^2\chi_{ij}\chi_{ij} + \frac{2}{3}l_{\mathrm{in}}^2\chi_{ij}\chi_{ji} \tag{13}$$

In Eq. (13), l_{SG} is the length scale associated with the invariant $\eta^{(1)}_{ijk}\eta^{(1)}_{ijk}$ containing only stretch gradients and l_{CS} is the length scale associated to the invariant $\chi_e^2 = \frac{2}{3}\chi_{ij}\chi_{ij}$ containing only rotation gradients. Recognizing $\varepsilon_e^2 = \frac{2}{3}\varepsilon'_{ij}\varepsilon'_{ij}$ and introducing a single length scale associated to plastic strains, (13) can be rewritten like

$$E^2 = \varepsilon_e^2 + l^2\left[\left(\frac{l_{\mathrm{SG}}}{l}\right)^2\eta^{(1)}_{ijk}\eta^{(1)}_{ijk} + \left(\frac{l_{\mathrm{CS}}}{l}\right)^2\chi_e^2 + \left(\frac{l_{\mathrm{in}}}{l}\right)^2\chi_{\mathrm{in}}^2\right] \tag{14}$$

Eq. (14) just expresses a particular coupling between the densities of statistically stored and geometrically necessary dislocations. Eq. (14) is useful, as will be seen shortly, because it allows the characterization of the model in terms of a single length scale. Subsequently we will refer to l as the plastic length scale. An analogous but more general coupling between the dislocation densities has been proposed by Abu Al-Rub and Voyiadjis (2004) as follows

$$E = \left\{\varepsilon_{\mathrm{e}}^{\gamma_1} + l^{\gamma_2}\left[\left(\frac{l_{\mathrm{SG}}}{l}\right)^{\gamma_2}\eta^{(1)}_{ijk}\eta^{(1)}_{ijk} + \left(\frac{l_{\mathrm{CS}}}{l}\right)^{\gamma_2}\chi_{\mathrm{e}}^{\gamma_2} + \left(\frac{l_{\mathrm{in}}}{l}\right)^{\gamma_2}\chi_{\mathrm{in}}^{\gamma_2}\right]\right\}^{1/\gamma_3} \tag{15}$$

where Eq. (15) reduces to Eq. (14) upon choosing $\gamma_1 = \gamma_2 = \gamma_3 = 2$. Abu Al-Rub and Voyiadjis (2004) have derived an analytical expression for the length scale l where it is shown that it is related to micromechanical physical parameters and specifically to the average spacing between the gliding dislocations. According to Abu Al-Rub and Voyiadjis (2004) l is given by

$$l = \left(\frac{\alpha_{\mathrm{G}}}{\alpha_{\mathrm{S}}}\right)^2\left(\frac{b_{\mathrm{G}}}{b_{\mathrm{S}}}\right)\overline{M}\bar{r}L_{\mathrm{S}} \tag{16}$$

In (16) αs are statistical coefficients which account for the deviation from regular spatial arrangements of the dislocations population, b is the magnitude of Burger's vector, L_{S} is the average spacing between statistically stored dislocations, $\bar{r}$ is the Nye's factor and $\overline{M}$ is the norm of Schmidt's orientation tensor. Based on Eq. (14) and on different phenomenological combinations of the length scales, different strain gradient plasticity theories have been formulated. Here we have chosen the combination of length scales corresponding to the Fleck and Hutchinson (1993) couple stress theory and defined as follows

$$l_2 = \frac{1}{2}l \quad \text{and} \quad l_3 = \sqrt{\frac{5}{24}}l \text{ leading to } l_{\mathrm{SG}} = 0, \quad l_{\mathrm{CS}}^2 = l^2, \quad l_{\mathrm{in}}^2 = 0 \quad \text{and} \quad E^2 = \varepsilon_e^2 + l_{\mathrm{CS}}^2\chi_e^2$$

This combination is suitable for bending applications where the strain gradient terms appear as curvatures or rotation gradients.

From Eq. (12) and the particular length scale combination shown above it can be seen that if l is known, l_{CS} can be determined, therefore fully characterizing the solid.

2.3. Length scale determination from nanoindentation experiments

Abu Al-Rub and Voyiadjis (in press) related the density of statistically stored dislocations to the indentation test parameters for conical and pyramidal indenters and have proposed the following model that directly yields the length scale from the nanoindentation experiment,

$$\left(\frac{H}{H_0}\right)^{\beta} = 1 + \left(\frac{h^*}{h_p}\right)^{\beta/2} \tag{17}$$

where $h^* = \varsigma l$ with $\varsigma = \frac{3}{2c\tilde{r}} \tan\theta$ and θ being the angle of indented surface that remains constant, H is the size dependent hardness, H_0 is the hardness at large indentation depths. The additional parameter for the length scale determination is $c = 0.4$ taken from Atkins and Tabor (1965). When the data corresponding to the indentation test is plotted like $(H/H_0)^{\beta}$ vs $(h)^{-\beta/2}$ the length scale parameter l can be identified from the slope $h^{*\beta/2}$. Since the size effects are expected to become important at very small indentation depths it is important to have reliable data at those scales. This is not only controlled by the sensitivity of the indenter but also the surface treatment and the environmental conditions during testing. Recently Gomez et al. (submitted for publication) used the described approach and performed a series of indentations in a set of solder joints obtained from actual microelectronic packages. The results show a consistent average value of 0.20 GPa for the macrohardness (i.e the H_0 in Eq. (17)). In that study indentations below 300 nm have been neglected due to uncertainties in the contact surface due to surface asperities and to the very nature of the material which makes the specimen preparation more difficult. Details of the experiments and sample preparation are presented there. Fig. 1 shows some results from the experimental study conducted by Gomez et al. (submitted for publication). The first part of the figure shows hardness vs indentation depth at different locations. The second part shows the data plotted like $(H/H_0)^{\beta}$ vs $(h)^{-\beta/2}$ for $\beta = 2$. In that study a batch of more than a hundred indentations on different solders was performed with very consistent results for the length scale parameter of the order of $l = 0.30$ μm. This value is consistent with other metallic materials reported in the literature like copper, nickel and aluminum.

3. Thermodynamics based constitutive model and finite element implementation

Damage is introduced into the model by making use of the effective stress concept and the strain equivalence principle as presented in Lemaitre (1996). The constitutive model evolution equations are first written for a rate independent material. In order to write the constitutive model evolution equations it is convenient to introduce the following elastic relationships corresponding to a reduced couple stress solid

$$\begin{aligned} \sigma &= C\varepsilon \\ l^{-1}m &= \widetilde{D} l\chi \end{aligned} \tag{18}$$

or more generally

$$\Sigma = ME \equiv \begin{bmatrix} C & 0 \\ 0 & \widetilde{D} \end{bmatrix} \begin{bmatrix} \varepsilon \\ l\chi \end{bmatrix} \tag{19}$$

where we have collapsed σ and $l^{-1}m$ and ε and $l\chi$ into Σ and E respectively and C and $\widetilde{D}$ are elastic constitutive matrices. Accordingly, Hooke's law after considering damage for a rate dependent material can be written as

$$\dot{\Sigma} = (1-D)M(\dot{E} - \dot{E}^{\mathrm{VP}} - \dot{E}^{\theta}) \tag{20}$$

where $\dot{E}^{\theta}$ is the thermal strain rate, $\dot{E}$ is the total strain rate and $\dot{E}^{\mathrm{VP}}$ is the viscoplastic strain rate and D represents the damage parameter. The elastic viscoplastic domain is defined according to the following yield function

$$F(\Sigma,\alpha) = \sqrt{\xi^{\mathrm{T}} P \xi} - \sqrt{\frac{2}{3}} K(\alpha) \tag{21}$$

where $\xi = \Sigma - X$ is a generalized relative stress vector with X being the back stress representing the displacement of the yield surface in the stress space. P is a constant matrix such that $P\xi$ gives the deviatoric component of ξ and $\sqrt{\frac{2}{3}\xi^{\mathrm{T}} P \xi}$ is the Von Mises equivalent stress for the generalized relative stress vector. $K(\alpha)$ represents the size of the yield surface or isotropic hardening component and it is a function of the hardening parameter α. Damage is included into the yield surface directly in the evolution of the hardening variables. The viscoplasticity is specified by the flow rule defining the direction of plastic flow and the hardening laws. Using associative normal plasticity we have

$$\dot{E}^{\mathrm{VP}} = \gamma \frac{P\xi}{(1-D)} \tag{22}$$

$$\dot{\alpha} = \sqrt{\frac{2}{3}} \gamma (1-D) \sqrt{\xi^{\mathrm{T}} P \xi} \tag{23}$$

$$\dot{X} = \gamma \frac{2}{3} H'(\alpha)(1-D)\xi \tag{24}$$

Note that in (24) the kinematic hardening modulus H' can be a non-linear function of the hardening parameter α. For the strain gradient theory, Eq. (24) implies that the couple backstress evolves in the same manner as the Cauchy stress components. The parameter γ is called the consistency parameter and it obeys the following Kuhn–Tucker complementarity conditions

$$\gamma \geqslant 0, \quad F(\Sigma,\alpha) \leqslant 0 \quad \text{and} \quad \gamma F(\Sigma,\alpha) = 0$$

in addition to the consistency condition

$$\gamma \dot{F}(\Sigma,\alpha) = 0$$

A material point is considered elastic if $F(\Sigma,\alpha) < 0$. Stress states such $F(\Sigma,\alpha) > 0$ are non-admissible. A material point is plastic when $F(\Sigma,\alpha) = 0$ and $\gamma > 0$ which is decided based on the consistency condition. In contrast to the rate independent case, in a viscoplastic material, states of stress such that $F(\Sigma,\alpha) > 0$ are admissible and the complementarity and consistency conditions are replaced by a constitutive equation for the consistency parameter

$$\gamma = \frac{1}{\eta} \langle \phi(F) \rangle \tag{25}$$

where η is a viscosity parameter and $\phi(F)$ is a predefined function of the yield surface where typical choices for metals and its alloys are exponentials and power laws. In (25) $\langle\,\rangle$ represents McCauley brackets. From (25) it follows that

$$F = \Theta\left(\frac{\eta\Delta\gamma}{\Delta t}\right) \tag{26}$$

where

$$\Theta\left(\frac{\eta\Delta\gamma}{\Delta t}\right) = \phi^{-1}\left(\frac{\eta\Delta\gamma}{\Delta t}\right)$$

Note in (25) and (26) that as $\eta \to 0$, $F \to 0$ and γ remains finite recovering the rate independent case. In the present model the assumed creep law is the one from Kashyap and Murty (1981) where the viscosity parameter and the overstress function have the following forms

$$\begin{aligned} \eta &= \frac{k\theta}{AD_0E^{n-1}b}\left(\frac{d}{b}\right)^p \mathrm{e}^{Q/R\theta} \\ \phi(F) &= F^n \end{aligned} \tag{27}$$

where A is a dimensionless material parameter which is temperature and rate dependent. $D_i = D_0\mathrm{e}^{-Q/R\theta}$ is a diffusion coefficient with D_0 representing a frequency factor, Q is the creep activation energy, R is the universal gas constant, θ is the absolute temperature in Kelvin $E(\theta)$ is a temperature dependent Young's modulus. b is the characteristic length of crystal dislocation (magnitude of Burger's vector) k is Boltzman's constant. d is the average grain size. p is a grain size exponent. n is a stress exponent.

This constitutive relationship has been used by Basaran and Tang (2002) and Basaran et al. (2004) and verified against experimental results on thin layer solder joints subjected to thermomechanical fatigue.

The isotropic hardening (or evolution of the radius of the yield surface) proposed by Chaboche (1989) is utilized

$$K(\alpha) = \sigma_{\mathrm{y}}^0 + Q_\infty(1 - \mathrm{e}^{-c\alpha}) \tag{28}$$

where σ_{y}^0 is the initial size of the yield surface. Q_∞ is a saturation value for the isotropic stress or asymptotic value of the yield surface c is a rate hardening coefficient.

From (22) and (23) it follows that $\dot{\alpha} = \|\dot{E}^{\mathrm{VP}}(t)\| \equiv \sqrt{\dot{\varepsilon}_{ij}^{\mathrm{VP}}\dot{\varepsilon}_{ij}^{\mathrm{VP}} + l^2\dot{\chi}_{ij}^{\mathrm{VP}}\dot{\chi}_{ij}^{\mathrm{VP}}}$, which agrees with the definition of equivalent viscoplastic strain rate. Considering the character of thegeneralized viscoplastic strain vector, it can be seen that the isotropic hardening is enhanced by the presence of the curvature invariant as proposed in the original theory of Fleck and Hutchinson (1993). This is considered as a measure of the density of geometrically necessary dislocations. Damage is considered following the approach by Basaran and Yan (1998), Basaran et al. (2004), Tang (2002), where the relation between the disorder and entropy and established by Boltzmann using statistical mechanics and the second law of thermodynamics is exploited. Their thermodynamic framework assumes that damage and the disorder are analogous concepts and the thermodynamic disorder can be used to model the damage evolution. The Damage evolution function is given by

$$D = (1 - \mathrm{e}^{-((\Delta e - \Delta\phi)/(N_0 k\theta/\overline{m}_s))})D_{\mathrm{cr}} \tag{29}$$

where D_{cr} is a damage threshold, which allows bridging a link between strain energy spent in the system and disorder. $\Delta e - \Delta\phi$ is the difference between the changes in the internal energy and the Helmholtz free energy with respect to a reference state. For the couple stress solid this difference is obtained as follows. For the couple stress solid the internal energy equation, which is an expression of the first law of thermodynamics, reads

$$\rho\frac{\mathrm{d}e}{\mathrm{d}t} = \sigma_{ij}^{\mathrm{S}}D_{ij}^{\mathrm{in}} + m_{ji}\chi_{ij} + \rho\hat{\gamma} - \hat{q}_{i,i} \tag{30}$$

where D_{ij}^{in} is the rate of deformation tensor. For the particular case of small strains and small displacements $D_{ij}^{\text{in}} = \frac{\mathrm{d}\varepsilon_{ij}^{\text{in}}}{\mathrm{d}t}$, $\hat{\gamma}$ is the internal heat production rate per unit mass and $\hat{q}_i$ is the rate of heat flux through the surface. The Helmholtz free energy for a Cosserat continuum is written in terms of the symmetric part of the Cauchy stress tensor since the elastic curvatures vanish, thus

$$\rho \frac{\mathrm{d}\psi}{\mathrm{d}t} = \sigma_{ij}^{\text{S}} D_{ij}^{\text{el}} \tag{31}$$

combining (30) and (31) yields the difference between the changes in the internal energy and the Helmholtz free energy with respect to a reference state in the presence of couple stresses.

$$\Delta e - \Delta\phi = \frac{1}{\rho}\int_{t_1}^{t_2} \sigma_{ij}^{\text{S}} D_{ij}^{\text{in}}\,\mathrm{d}t + \frac{1}{\rho}\int_{t_1}^{t_2} \mu_{ji}\chi_{ij}\,\mathrm{d}t + \int_{t_1}^{t_2} \gamma\,\mathrm{d}t - \int_{t_1}^{t_2} q_{i,i}\,\mathrm{d}t \tag{32}$$

Within the finite element method the solution is developed by a series of small increments with the solution at every increment found by a Newton method. During every increment the problem may be regarded as strain driven in the following sense. At the beginning of the time step the total and viscoplastic strain fields and the internal state variables are considered to be known. Assuming the incremental displacement $\Delta\vec{u}$ to be given, the basic problem is to update the field variables to their values at the end of the time step in a manner consistent with the constitutive model described above.

The constitutive model just described is integrated using a return mapping algorithm as presented in Simo and Hughes (1998). A Backward-Euler scheme yields the following set of algorithmic equations corresponding to Eqs. (22)–(24)

$$E_{n+1} = E_n + \Delta E_{n+1} \tag{33}$$

$$\alpha_{n+1} = \alpha_n + \Delta\gamma(1-D)\sqrt{\frac{2}{3}\xi_{n+1}^{\text{T}} P \xi_{n+1}} \tag{34}$$

$$X_{n+1} = X_n + \Delta\gamma\frac{2}{3}H'(1-D)\xi_{n+1} \tag{35}$$

The standard operator split technique defines the following trial state

$$\Sigma_{n+1}^{\text{tr}} = \Sigma_n + (1-D)M\Delta E_{n+1} \tag{36}$$

using (36) and Hooke's law (20) we can write

$$\Sigma_{n+1} = \Sigma_{n+1}^{\text{tr}} - M\Delta\gamma P\xi_{n+1} \tag{37}$$

$$\xi_{n+1}^{\text{tr}} = \Sigma_{n+1}^{\text{tr}} - X_n \tag{38}$$

from (37) and (38) an updated relative stress can be obtained in terms of the algorithmic consistency parameter $\Delta\gamma$:

$$\xi_{n+1} = \Xi(\Delta\gamma)\frac{1}{1+\frac{2}{3}H'\Delta\gamma(1-D)}M^{-1}\xi_{n+1}^{\text{tr}} \tag{39}$$

where

$$\Xi(\Delta\gamma) = \left[M^{-1} + \frac{\Delta\gamma P}{1+\frac{2}{3}H'(1-D)\Delta\gamma}\right]^{-1} \tag{40}$$

The consistency parameter $\Delta\gamma$ is obtained from the yield criteria and the corresponding constitutive model given in Eqs. (25) and (27). Thus

$$F(\Delta\gamma) - \Theta\left(\frac{\eta\Delta\gamma}{\Delta t}\right) \equiv \hat{f}_{n+1} - \sqrt{\frac{2}{3}}K(\alpha_{n+1}) - \Theta\left(\frac{\eta\Delta\gamma}{\Delta t}\right) = 0 \tag{41}$$

where $\hat{f}_{n+1} = [\xi^{\mathrm{T}}_{n+1} P \xi_{n+1}]^{1/2}$ and $\Theta(\frac{\eta\Delta\gamma}{\Delta t}) = \phi^{-1}(\frac{\eta\Delta\gamma}{\Delta t})$ as defined in the previous section. Eq. (41) is a scalar non-linear equation in the consistency parameter $\Delta\gamma$, which can be solved by a local Newton iteration. In the Newton–Raphson iteration scheme the elastoplastic tangent modulus consistent with the integration scheme is needed in order to preserve the convergence properties of the Newton algorithm. Linearizing the above set of algorithmic equations yields

$$\frac{\mathrm{d}\Sigma_{n+1}}{\mathrm{d}E_{n+1}} = (1-D)\left(\Xi(\Delta\gamma) - \frac{1}{(1+\beta)} N \otimes N\right) \tag{42}$$

where

$$N = \frac{\Xi(\Delta\gamma) P \xi_{n+1}}{\sqrt{\xi^{\mathrm{T}}_{n+1} P \Xi(\Delta\gamma) P \xi_{n+1}}}$$

$$\beta = \left[(1-D)\frac{2\theta_1}{3\theta_2}\hat{f}^2_{n+1}(K'\theta_1 + H'\theta_2) + \frac{\theta_1^2}{\theta_2}\frac{\mathrm{d}\Theta}{\mathrm{d}\Delta\gamma}\hat{f}_{n+1}\right]\frac{1}{\xi^{\mathrm{T}}_{n+1} P \Xi(\Delta\gamma) P \xi_{n+1}}$$

$$\theta_1 = 1 + \frac{2}{3}H'(1-D)\Delta\gamma$$

$$\theta_2 = 1 - \frac{2}{3}K'(1-D)\Delta\gamma$$

In order to implement the model within the framework of the finite element method we follow the approach of Shu and Fleck (1999) where we treat the rotation ω as an independent degree of freedom and enforce the kinematic constraint given by Eq. (1) by a penalty function method. Therefore we can use elements of C_0 continuity. The asymmetric shear stress τ_{ij} is related to the relative rotation tensor α_{ij} through a penalty number G_a and the enhanced principle of virtual work accounting for the kinematic constrain reads as

$$\int_\Omega \sigma_{ij}\delta\varepsilon_{ij}\mathrm{d}\Omega + \int_\Omega m_{ij}\delta\chi_{ij}\mathrm{d}\Omega + \int_\Omega G_a\alpha_{ij}\delta\alpha_{ij}\mathrm{d}\Omega - \int_{\partial\Omega} t_i\delta u_i\mathrm{d}\Gamma - \int_{\partial\Omega} q_i\delta\omega_i\mathrm{d}\Gamma = 0 \tag{43}$$

or using matrix notation

$$\int_V \delta E^{\mathrm{T}}\Sigma\,\mathrm{d}V + \int_V G_a\delta\alpha^{\mathrm{T}}\alpha\,\mathrm{d}V - \int_S \delta\bar{u}^{\mathrm{T}}\bar{t}\,\mathrm{d}S = 0 \tag{44}$$

We have implemented the above framework into the commercial finite element code ABAQUS by means of its user element subroutine capabilities. The overall algorithm for implementing the user element and the constitutive model integration scheme are provided in the Appendix A. In ABAQUS the problem is solved using a Newton–Raphson scheme.

4. Numerical analysis and results

We have performed two sets of analysis. First the model has been tested on the microbending experimental results reported by Stolken and Evans (1998). Second, we have used the damage mechanics viscoplastic constitutive model to apply cyclic loads on a Pb/Sn thin layer solder joint cantilever having the same thick-

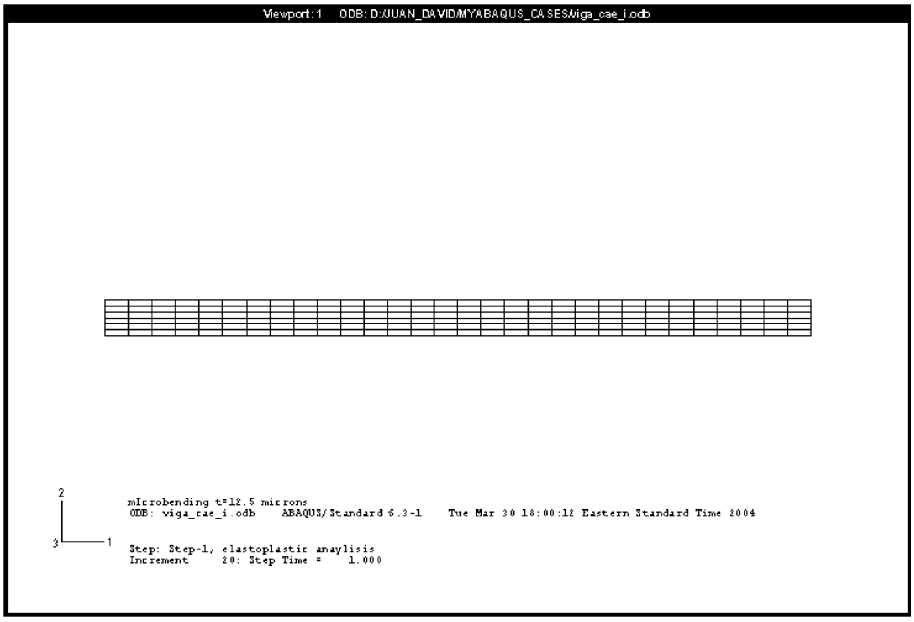

Fig. 3. Finite element mesh of cantilever beam.

Table 1
Material parameters used in the constitutive model

Material parameters	
Young's modulus (Gpa)	$52.10–0.1059\theta$
Shear modulus (Gpa)	$19.44–0.0395\theta$
Isotropic hardening parameters	
R_{00} (Mpa)	$37.47–0.0748\theta$
C	383.3
Kinematic hardening parameters	
σ_y (Mpa)	$60.069–0.140\theta$
X_{00} (Mpa)	13.6
γ	457.9
Flow rule parameters	
A	7.6×10^9
D_0 (mm^2/s)	48.8
b (mm)	3.18×10^{-7}
d (mm)	10.6×10^{-3}
N	1.67
P	3.34
Q (mJ/mol)	44.7×10^6

ness as Stolken and Evans (1998) specimens. This analysis was intended to test the stability of the computational framework under cyclic loading conditions. A typical finite element discretization using 9-noded user defined elements for both sets of analysis is shown in Fig. 3. This mesh shows a good convergency rate at least under elastic conditions. The material properties used in the viscoplastic model are shown in Table 1.

4.1. Simulation of the microbending experiment

Stolken and Evans (1998) performed microbending experiments on thin nickel foils in order to determine the material length scale. Their experimental results have been used to validate several computational models like in Gao and Huang (2001), Chen and Wang (2000), Wang et al. (2003). Their experiment may now be considered a benchmark. They studied microbeams with thickness of 12.5, 25.0 and 50.0 μm. The

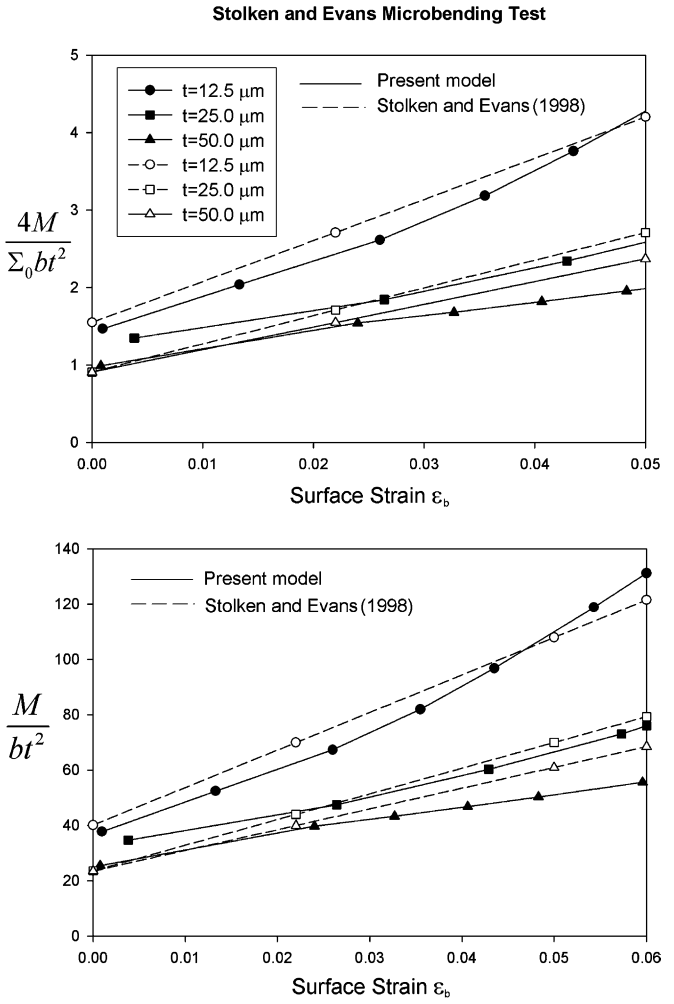

Fig. 4. Stolken and Evans (1998) microbending experimental results on nickel foils compared to present model. $l = 5.0$ μm, $E = 220.0$ GPa, $\Sigma_0 = 103$ MPa.

specimens were placed in a fixture used to impose curvatures by means of a set of wires of given diameter. Next, using a confocal microscope they measured the residual plastic curvature and recovered curvature upon unloading. Since the unloading is elastic, the recovered curvature can be used to determine the corresponding bending moment. They presented their results in terms of two normalized descriptions of the moment vs surface strain ε_b. First, they used M/bt^2 where t is the beam thickness. This measure is obtained directly out of the experiment. Second they used $4M/\Sigma_0 bt^2$, where Σ_0 is the yield strength of the material from a uniaxial tension test. This quantity is meaningful within the Fleck and Hutchinson (1997) framework, which was used to obtained the material length scale. A comparison of Stolken and Evans (1998) results with our computational model are presented in Fig. 4 along with the used material parameters. We have used the same material properties obtained in their testing. In both data sets it can bee seen how the size effects are more important for the thinner beams. It should be pointed out that when the

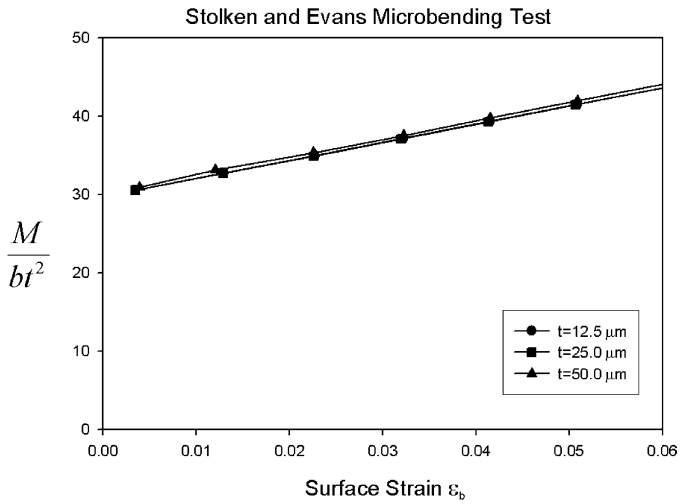

Fig. 5. Finite element simulation of Stolken and Evans (1998) tests using a classical plasticity theory model. $l = 0.0\ \mu m$, $E = 220.0$ GPa, $\Sigma_0 = 103$ MPa.

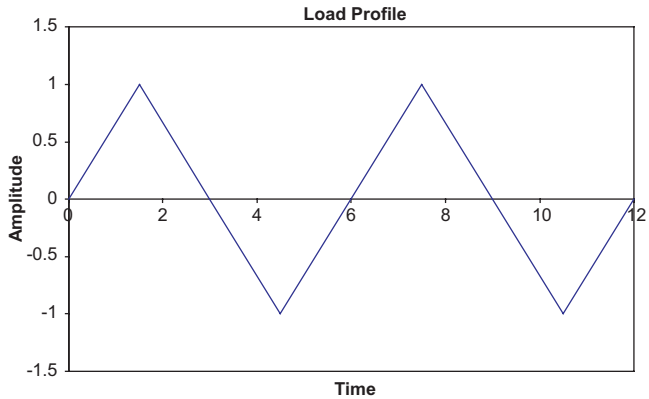

Fig. 6. Load history profile.

length scale is made equal to zero the results for the three beams superimpose to each other as shown in Fig. 5. Comparisons between experimental data and finite element simulations prove that the proposed model is very effective.

4.2. Pb/Sn thin layer solder joint in bending

Here, the constitutive framework is applied to simulate the response of a thin layer solder joint (surface mount technology type) under cyclic loading conditions using the material properties from Tang (2002) and

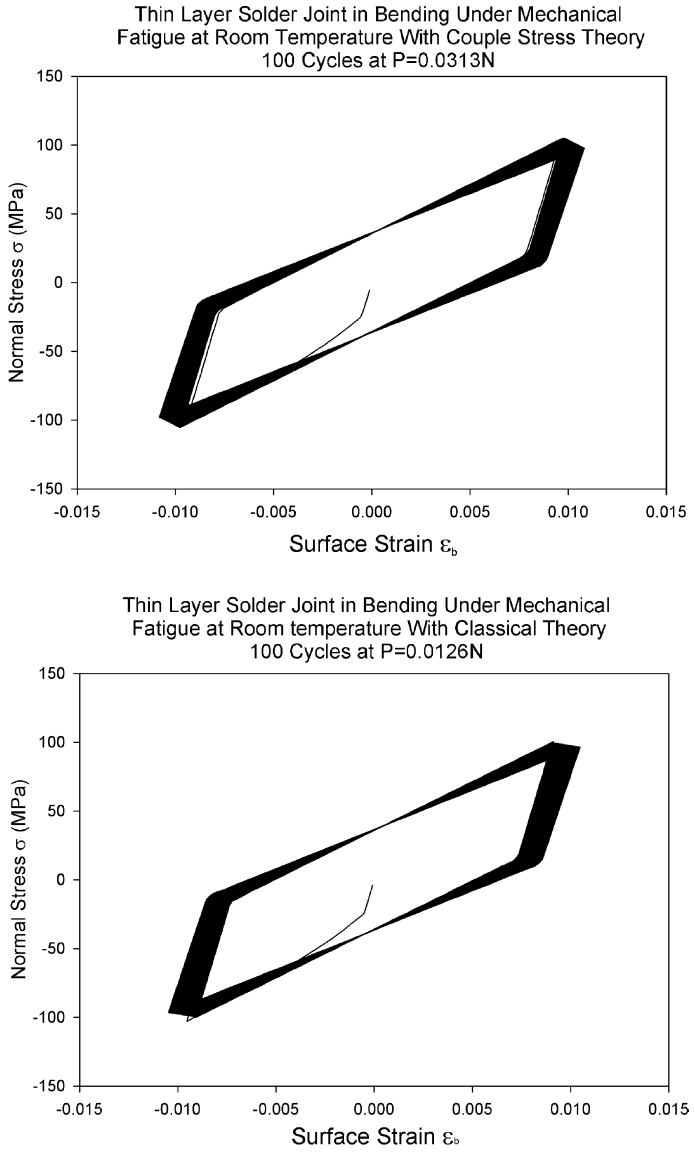

Fig. 7. Couple stress and classical theory solutions with different load for a 12.5 μm thickness beam and $l = 5.0$ μm and $l = 0.0$ μm.

reported in Table 1. Load time history is shown in Fig. 6. First, we studied a 12.5 μm thick solder layer under a cyclic tip load using classical theory (i.e., $l = 0.0$) and the couple stress theory with different assumed values of the length scale. Results are shown in Figs. 7 and 8. In the analysis considered we applied 100 load cycles at room temperature. For a given load and using the couple stress theory we determined the equivalent load that would produce the same response as in the classical model. The relation between the two loads is close to the one obtained, between the moment measured by Stolken and Evans (1998) and that predicted by classical theory. Next, we performed the same analysis using the strain gradient theory but

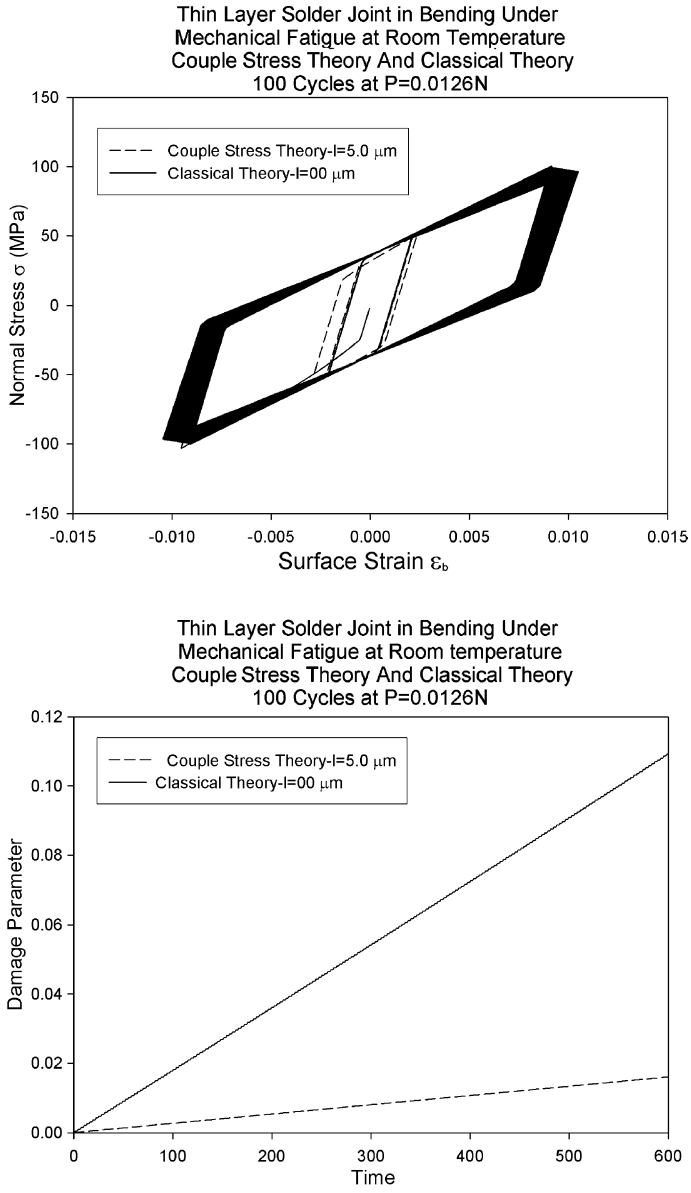

Fig. 8. Classical and couple stress theory solution with same load $l = 5.0$ μm and $l = 0.0$ μm.

using the load from the classical model. The introduction of the length scale affects both the stress-strain response and the evolution of the damage parameter. This means that when the material size effects are considered into the model the number of cycles to attain a given damage value is larger as compared to the classical theory. To study the influence of the length scale, the same analysis was repeated with three dif-

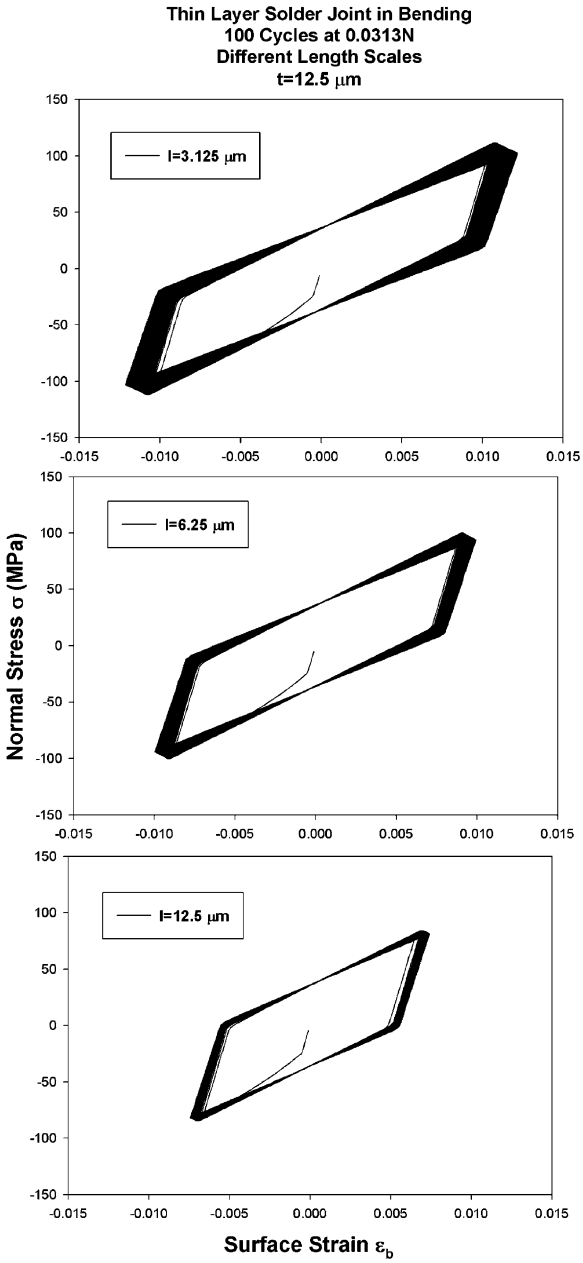

Fig. 9. Couple stress theory solution with different length scales for a 12.5 μm thickness beam.

ferent length scales. Normal stress vs surface strain results are shown in Fig. 9. The influence of the length scale in the damage parameter (as defined by Eq. (29)) can be seen in Fig. 10. The previous analysis was extended to the case of 25.0 and 50.0 μm thickness beams. It can be seen in Figs. 11–18 that the size effects are stronger for the 12.5 μm thick beam and decrease in the direction of increasing thickness. Simulation results indicate that fatigue life is significantly affected by material length scale.

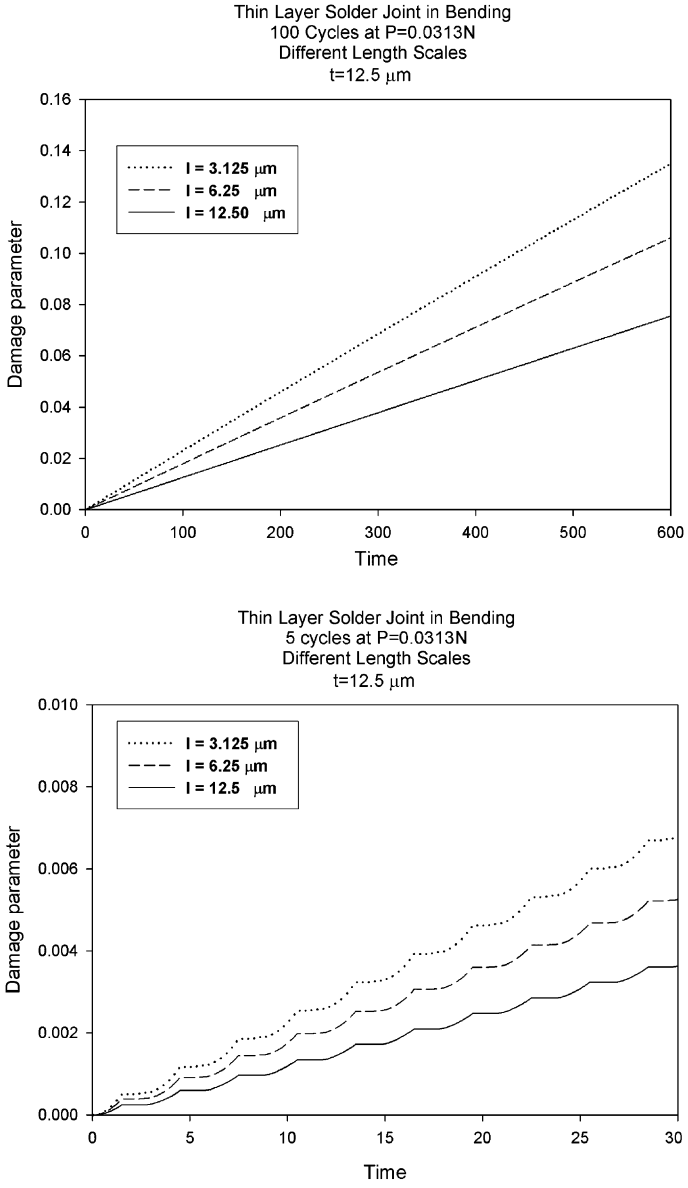

Fig. 10. Couple stress theory solution with different length scales for a 12.5 μm thickness beam.

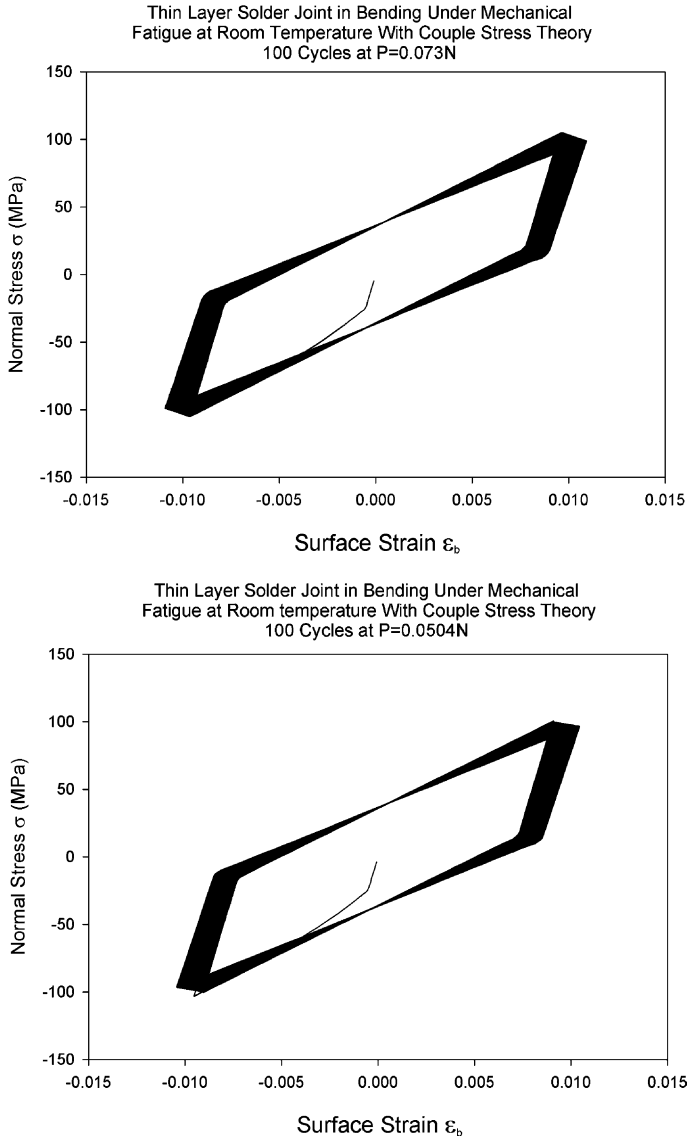

Fig. 11. Couple stress and classical theory solutions with different load for a 25.0 μm thickness beam $l = 5.0$ μm and $l = 0.0$ μm.

5. Conclusions

We have extended the Fleck and Hutchinson (1993) phenomenological strain gradient plasticity theory into flow theory to embed our damage mechanics based viscoplastic constitutive model to study the size dependent fatigue response of Pb/Sn solder joints under mechanical cycling loading. The model has been implemented into the commercial finite element code ABAQUS by a user element subroutine UEL. The corresponding algorithm for implementing the model is provided in the Appendix A.

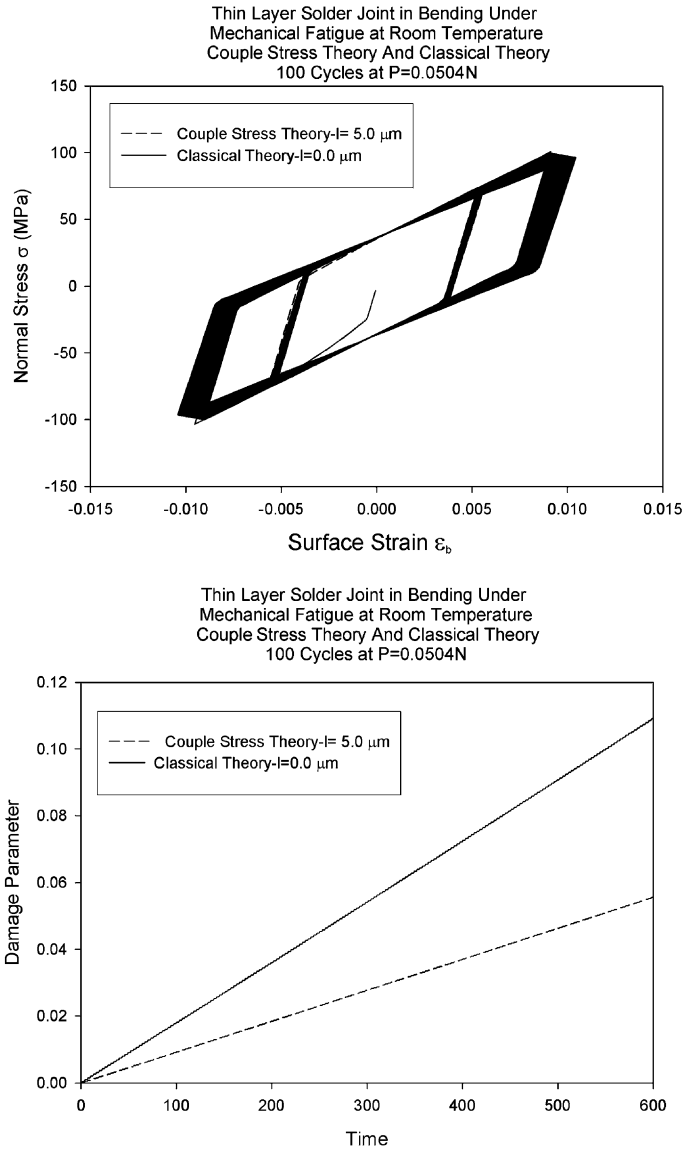

Fig. 12. Couple stress and classical theory solutions with same load for a 25.0 μm thickness beam $l = 5.0$ μm and $l = 0.0$ μm.

The model has been verified with the experimental results of Stolken and Evans (1998) on microbending of thin nickel foils. Good agreement between the computational model and the experimental data is obtained which suggest that the proposed model is robust. The model has also been used to simulate the behavior of a surface mount technology viscoplastic solder alloy beam under fatigue in bending. The length scale effect in damage has been shown to reduce the number of cycles to produce a given damage value as predicted with classical theory. In other words an increase in the fatigue life as the beam gets thinner. The conducted simulations have been performed under isothermal conditions and the constitutive model takes into account rate dependent effects as exhibited by solder alloys.

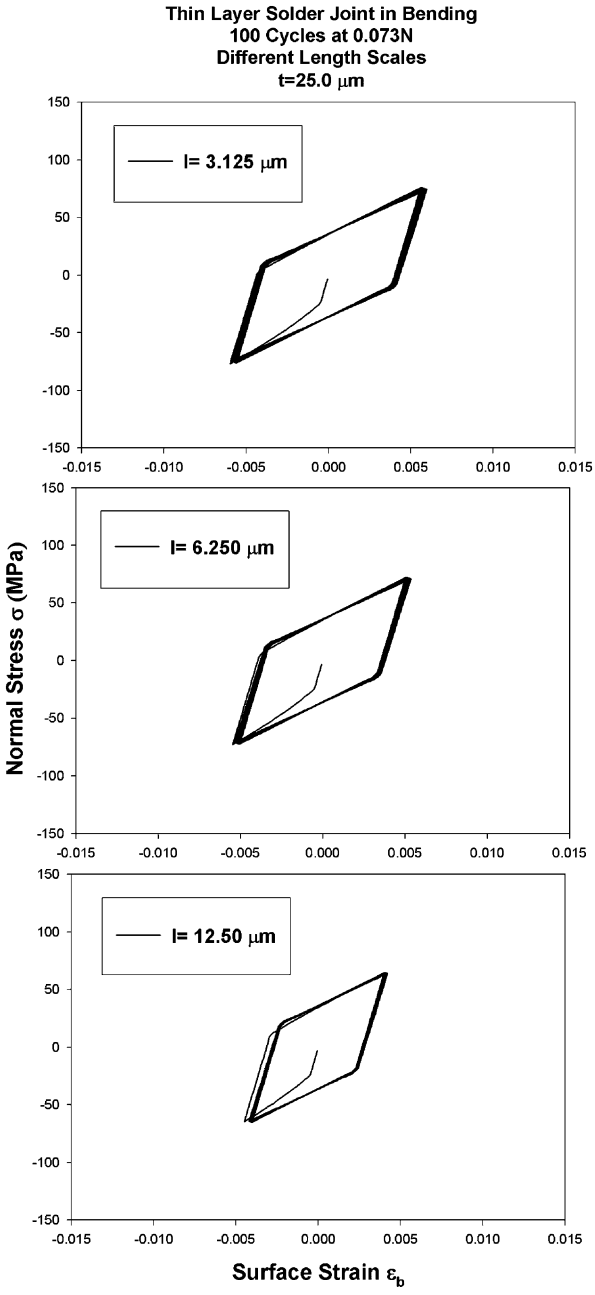

Fig. 13. Couple stress theory solution with different length scales for a 25.0 μm thickness beam.

Appendix A. User subroutines

User element implementation scheme (UEL.f)

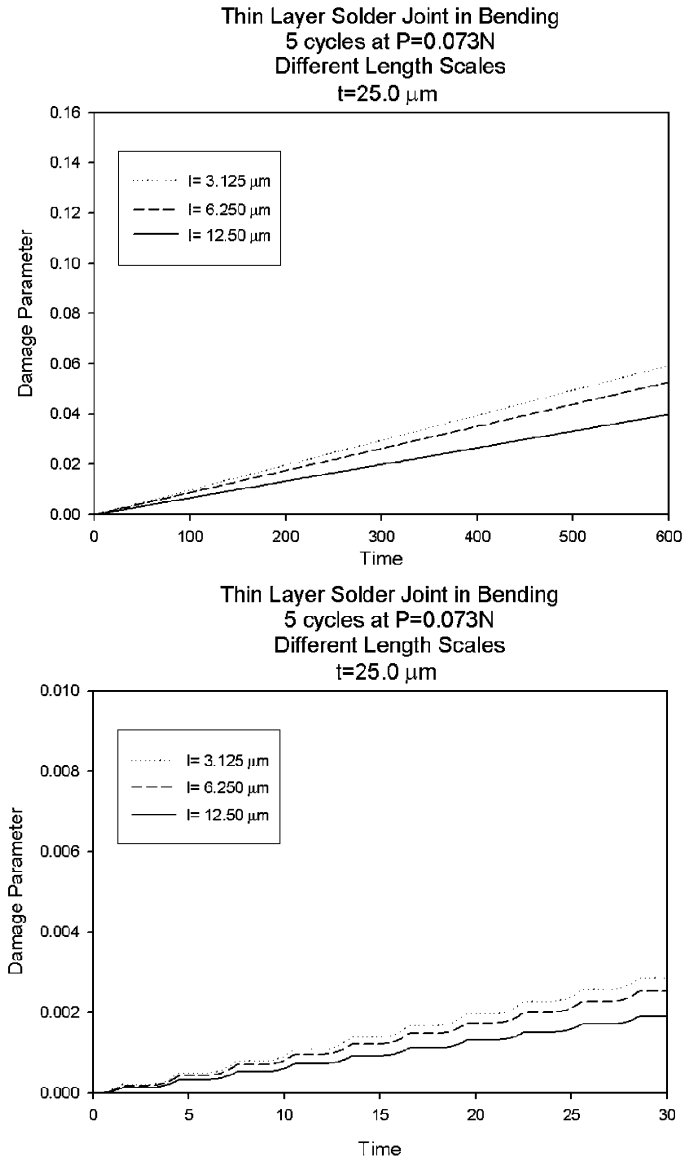

Fig. 14. Couple stress theory solution with different length scales for a 25.0 μm thickness beam.

Let $T \leftarrow 0(time)$
1 Assume ${}^{t}u, {}^{t}E, {}^{t}\Sigma, {}^{t}\kappa$ known.
2 Assemble ${}^{t+\Delta t}F_{\text{ext}} = \int_S N^{\mathrm{T}\,t+\Delta t}\bar{t}\,\mathrm{d}S$
Initialize ${}^{t+\Delta t}u^{(0)} \leftarrow {}^{t}u$ and ${}^{t+\Delta t}E^{(0)} \leftarrow {}^{t}E$
Let $i \leftarrow 0$, $Flag \leftarrow 0$
Do_While $Flag = 0$
$i \leftarrow i + 1$
(ABAQUS calls user subroutine UEL.f)

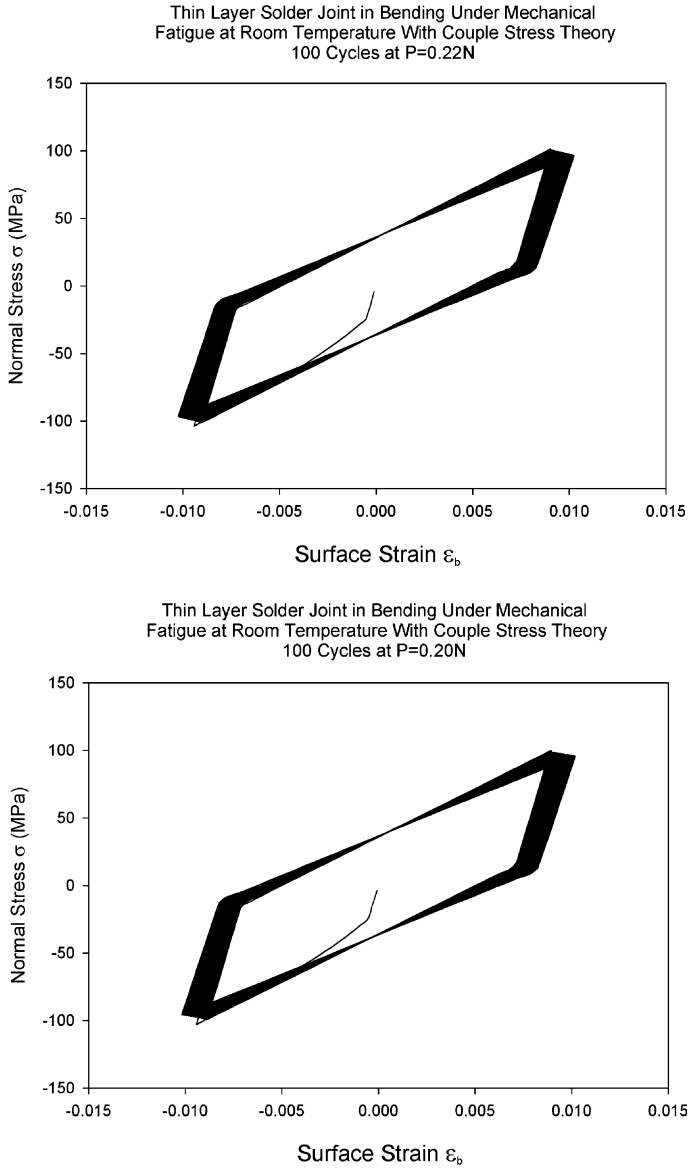

Fig. 15. Couple stress and classical theory solutions with different load for a 50.0 μm thickness beam $l = 5.0$ μm and $l = 0.0$ μm.

Assemble B_E, B_α
Call UMAT.f to compute

$${}^{t+\Delta t}\Sigma^{(i-1)}, {}^{t+\Delta t}\kappa^{(i-1)}, {}^{t+\Delta t}C^{(i-1)}, {}^{t+\Delta t}D^{(i-1)}$$

Assemble ${}^{t+\Delta t}K^{(i-1)}$
Assemble residual (RHS)

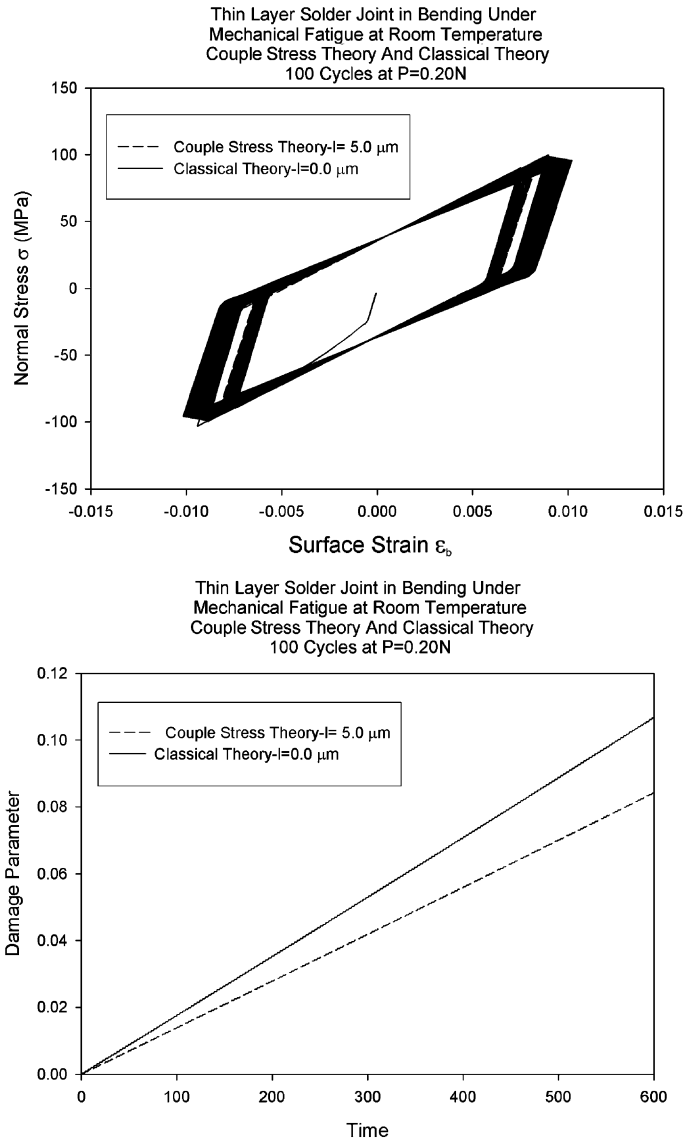

Fig. 16. Couple stress and classical theory solutions with same load for a 50.0 μm thickness beam $l = 5.0$ μm and $l = 0.0$ μm.

$$ {}^{t+\Delta t}F^{(i-1)} \leftarrow {}^{t+\Delta t}F_{\text{ext}} - \int_V B_E^{\mathrm{T}\,t+\Delta t}\Sigma^{(i-1)}\,\mathrm{d}V - \int_V B_\alpha^{\mathrm{T}\,t+\Delta t}\tau^{(i-1)}\,\mathrm{d}V $$

(Exits user subroutine UEL.f and returns to ABAQUS)

Solve ${}^{t+\Delta t}K^{(i-1)}\Delta u^{(i)} = {}^{t+\Delta t}F^{(i-1)}$

Update

$$ {}^{t+\Delta t}u^{(i)} \leftarrow {}^{t+\Delta t}u^{(i-1)} + \Delta u^{(i)} $$

$$ {}^{t+\Delta t}E^{(i)} \leftarrow B^{t+\Delta t}E^{(i)} $$

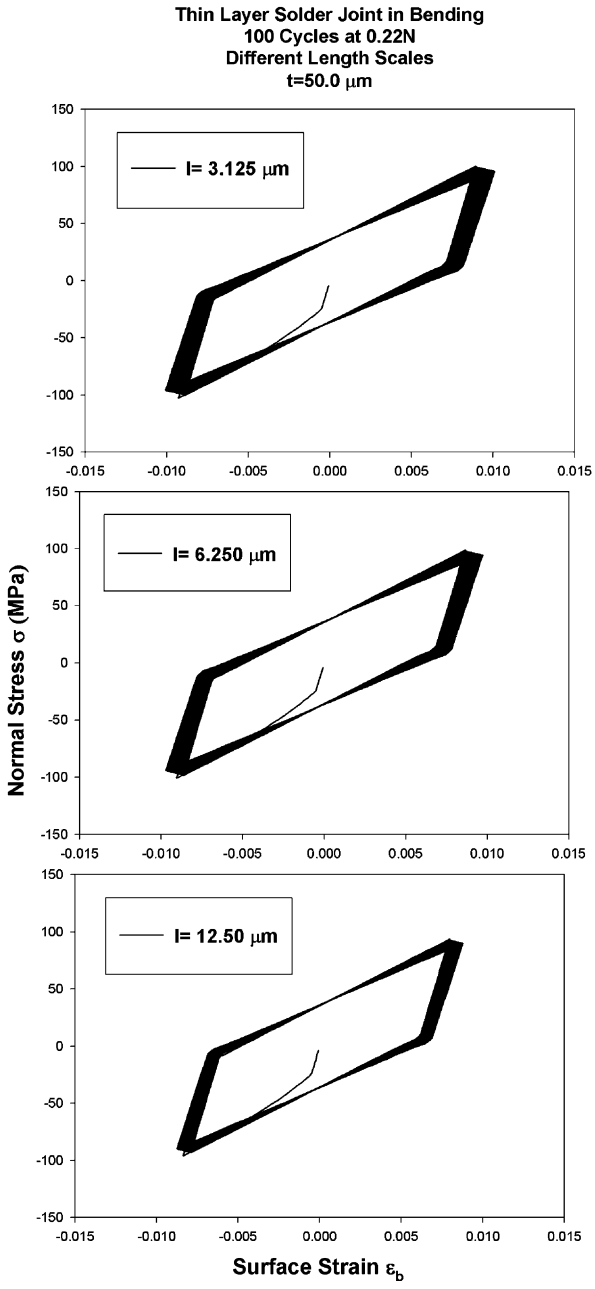

Fig. 17. Couple stress theory solution with different length scales for a 50.0 μm thickness beam.

If $\|error\| < tol$ **Then** $Flag \leftarrow 1$
End_Do_While
Let $\bar{T} \leftarrow \bar{T} + \Delta T$
If $T < T_{\max}$ **Then Goto step 2**
Analysis Complete

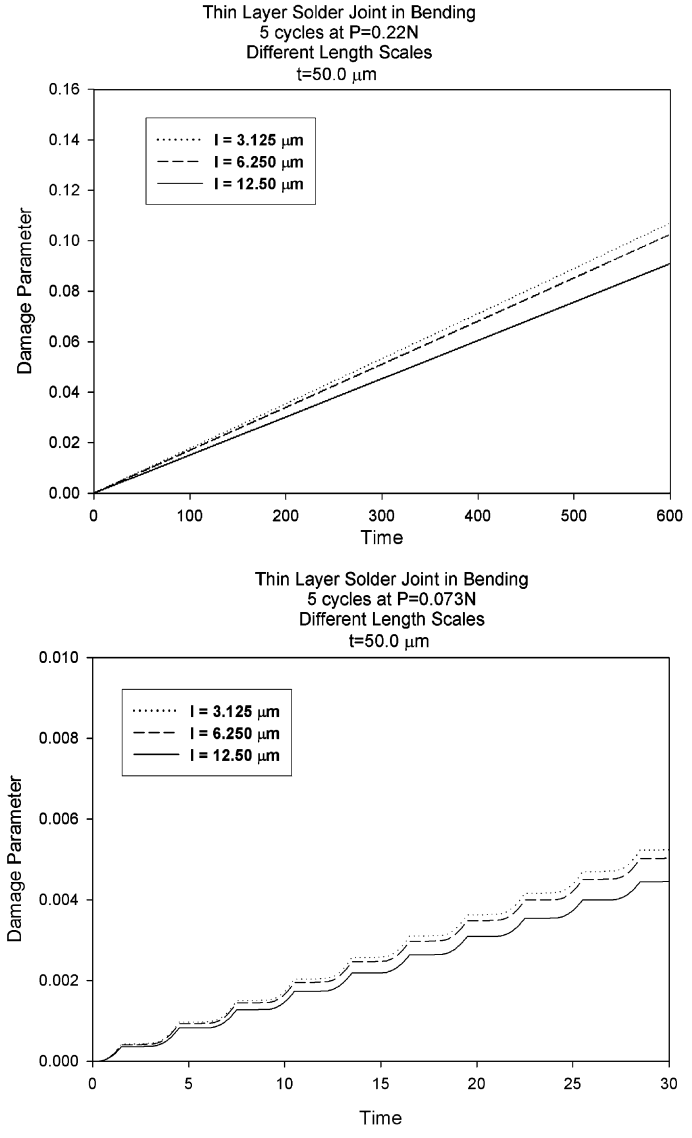

Fig. 18. Couple stress theory solution with different length scales for a 50.0 μm thickness beam.

Constitutive model integration scheme (UMAT.f)

Update strain $E_{n+1} = E_n + \nabla\Delta u$

Compute trial state $\Sigma^{\mathrm{tr}}_{n+1} = (1-D)M(E_{n+1} - E^{\mathrm{VP}}_n - E^{\theta}_{n+1})$

$\xi^{\mathrm{tr}}_{n+1} = \Sigma^{\mathrm{tr}}_{n+1} - X_n$

Compute trial yield function $F^{\mathrm{tr}}_{n+1} = \sqrt{\xi^{\mathrm{trT}}_{n+1} P \xi_{n+1}} - \sqrt{\frac{2}{3}} K(\alpha_n)$

IF $F_{n+1}^{\mathrm{tr}} > 0$ **THEN**

Call Newton local and solve $f(\Delta\gamma) = 0$ for $\Delta\gamma$

Compute $\Xi(\Delta\gamma) = \left[M^{-1} + \frac{\Delta\gamma P}{1+\frac{2}{3}H'(1-D)\Delta\gamma}\right]^{-1}$

Update $\xi_{n+1} = \Xi(\Delta\gamma)\frac{1}{1+\frac{2}{3}H'(1-D)\Delta\gamma}M^{-1}\xi_{n+1}^{\mathrm{tr}}$

$X_{n+1} = X_n + \Delta\gamma\frac{2}{3}H'(1-D)\xi_{n+1}$

$\Sigma_{n+1} = \xi_{n+1} + X_{n+1}$

$\alpha_{n+1} = \alpha_n + \Delta\gamma(1-D)\sqrt{\frac{2}{3}\xi_{n+1}^{\mathrm{T}}P\xi_{n+1}}$

$E_{n+1}^{\mathrm{VP}} = E_n^{\mathrm{VP}} + \Delta\gamma\frac{P\xi_{n+1}}{(1-D)}$

$E_{n+1}^{e} = E_{n+1} - E_{n+1}^{\mathrm{VP}} - E_{n+1}^{\theta}$

Compute consistent Jacobian $\frac{\mathrm{d}\Sigma_{n+1}}{\mathrm{d}E}_{n+1} = (1-D)\left[\Xi(\Delta\gamma) - \frac{1}{(1+\beta)}N\otimes N\right]$

ELSE

Elastic step (EXIT)

END IF

EXIT

References

Abu Al-Rub, R., Voyiadjis, G., 2004. Analytical and experimental determination of the material intrinsic length scale of strain gradient plasticity theory from micro- and nano-indentation experiments. Int. J. Plasticity 20, 1139–1182.

Abu Al-Rub, R., Voyiadjis, G., in press. Determination of the material intrinsic length scale of gradient plasticity theory. Int. J. Multiscale Computat. Eng.

Atkins, A.G., Tabor, D.T., 1965. Plastic indentation in metals with cones. J. Mech. Phys. Solids 13, 149–164.

Basaran, C., Tang, H., 2002. Implementation of a thermodynamic framework for damage mechanics of solder interconnect in microelectronic packaging. Proceedings of IMECE, 2002 ASME International Mechanical Engineering Congress and Exposition. New Orleans, LA.

Basaran, C., Yan, C., 1998. A Thermodynamic framework for damage mechanics of solder joints. J. Electron. Packag. Trans. ASME 120, 379–384.

Basaran, C., Zhao, Y., Tang, H., Gomez, J., 2004. A damage mechanics based unified constitutive model for Pb/Sn solder alloys. ASME Journal of Electronic Packaging (in press).

Begley, M., Hutchinson, J.W., 1998. The mechanics of size dependent indentation. J. Mech. Phys. Solids 46 (10), 2049–2068.

Bonda, N., Noyan, C., 1996. Effect of specimen size in predicting the mechanical properties of PbSn solder alloys. IEEE Trans. Compon. Packag. Manufact. Technol.—Part A 19 (2).

Chaboche, J., 1989. Constitutive equations for cyclic plasticity and viscoplasticity. Int. J. Plasticity 3, 247–302.

Chen, S., Wang, T., 2000. Anew hardening law fro strain gradient plasticity. Acta Mater. 48, 3997–4005.

Cosserat, E., Cosserat, F., 1909. Theorie des Corps Deformables. A Hermann & Fils, Paris.

de Borst, R., 1993. A generalization of J2-flow Theory for polar continua. Comput. Meth. Appl. Mech. Eng. 103, 347–362.

Fleck, N., Hutchinson, J., 1993. A phenomenological theory for strain gradient effects in plasticity. J. Mech. Phys. Solids 41 (12), 1825–1857.

Fleck, N., Hutchinson, J., 1997. Strain Gradient Plasticity. Adv. Appl. Mech. 33, 295–361.

Fleck, N., Muller, G., Ashby, M., Hutchinson, J., 1994. Strain gradient plasticity: Theory and experiment. Acta. Metall. Mater. 42 (2), 475–487.

Gao, H., Huang, Y., 2001. Taylor-based nonlocal theory of plasticity. Int. J. Solids Struct. 38, 2615–2637.
Gomez, J., Basaran, C., Ye, H., submitted for publication. Determination of the strain gradient plasticity length scale for microelectronics solder alloys. Int. J. Solids Struct.
Herrmann, L.R., 1983. Mixed finite elements for couple-stress analysis. In: Atluri, N.S., Gallagaher, H., Zienkiewicz, O. (Eds.), Mixed and Hybrid Finite Element Methods. John Wiley and Sons.
Kashyap, B., Murty, G., 1981. Experimental constitutive relations for the high temperature deformation of a Pb–Sn eutectic alloy. Mater. Sci. Eng. 50, 205–213.
Lemaitre, J., 1996. A Course on Damage Mechanics. Springer-Verlag, Germany.
Lloyd, D., 1994. Particle reinforced aluminum and magnesium matrix composites. Int. Mater. Rev. 39, 1–23.
McElhaney, K., Vlassak, J., Nix, W., 1998. Determination of indenter tip geometry and indentation contact area for depth-sensing indentation experiment. J. Mater. Res. 13, 1300–1306.
Mindlin, R., 1964. Micro-structure in linear elasticity. Arch. Ration. Mech. Anal. 16, 51–78.
Mindlin, R., 1965. Second gradient of strain and surface tension in linear elasticity. Int. J. Solids Struct. 1, 417–438.
Nix, W., Gao, H., 1998. Indentation size effects in crystalline materials: a law for strain gradient plasticity. J. Mech. Phys. Solids 46 (3), 411.
Nye, J., 1953. Some geometrical relations in dislocated crystals. Acta Metall. 1, 153–162.
Pamin, J., 1994. Gradient-dependent plasticity in numerical simulation of localization phenomena. PhD Dissertation, Delft University of Technology, The Netherlands.
Poole, W., Ashby, M., Fleck, N., 1996. Micro-hardness of annealed and work-hardened of copper polycrystals. Scrip. Mettall. Mater. 34 (4), 559–564.
Shrotriya, P., Allameh, S., Lou, J., Buchheit, T., 2003. On the measurement of the plasticity length scale parameter in LIGA nickel foils. Mech. Mater. 35, 235.
Shu, J.Y., Fleck, N.A., 1999. Strain gradient plasticity: size-dependent deformation of bicrystals. J. Mech. Phys. Solids 47, 297–324.
Simo, J., Hughes, T., 1998. Computational Inelasticity. Interdisc. Appl. Math. Springer.
Smyshlyaev, V., Fleck, N., 1996. The role of strain gradients in the grain size effects for polycrystals. J. Mech. Phys. Solids 44 (4), 465–495.
Stolken, J., Evans, A., 1998. A microbend test method for measuring the plasticity length scale. Acta. Mater. 14, 5109–5115.
Tang, H., 2002. A thermodynamic damage mechanics theory and experimental verification for thermomechanical fatigue life prediction of microelectronics solder joints. PhD Dissertation, University at Buffalo, The State University of New York.
Toupin, R., 1962. Elastic materials with couple-stresses. Arch. Rational Mech. Anal. 11, 385–414.
Wang, W., Huang, Y., Hsia, K., Hu, K., Chandra, A., 2003. A study of microbend test by strain gradient plasticity. Int. J. Plasticity 19, 365–382.
Xia, Z., Hutchinson, J., 1996. Crack tip fields in strain gradient plasticity. J. Mech. Phys. Solids 44 (10), 162–1648.
Xue, Z., 2001. The strain gradient effect on material behavior at the micron and submicron scales. PhD Dissertation, University of Illinois at Urbana-Champaign, 2001.
Xue, Z., Huang, Y., Li, M., 2001. Particle size effect in metallic materials: a study by the theory of mechanism-based strain gradient plasticity. Acta Mater. 50, 149–160.
Yuan, H., Chen, J., 2001. Identification of the intrinsic material length scale in gradient plasticity theory from macro-indentation tests. Int. J. Solids Struct. 38, 8171–8187.